Flow and heat transfer in a rotating cavity with a radial inflow of fluid

Part 1: The flow structure

M. Firouzian, J. M. Owen, J. R. Pincombe and R. H. Rogers*

Flow visualization has been conducted in a rotating cavity, comprising two steel discs and a peripheral polycarbonate shroud, for dimensionless flow rates of air up to $|C_w| \simeq 8000$ and rotational Reynolds number up to $Re_\phi \simeq 10^6$. For all the experiments, the ratio of the inner to outer radii of the discs was 0.1 and the ratio of the axial clearance between the discs to their outer radii was 0.133; five different shroud geometries were tested. The flow visualization has confirmed that the flow structure comprises a source region near the shroud, laminar or turbulent Ekman layers on the discs, a sink layer near the centre of the cavity, and an interior core of rotating fluid. Above a certain flow rate, this structure was found to be unstable; heating one disc tended to stabilize the flow. For isothermal flow, measurements of the size of the source region were in good agreement with values predicted from a simple theoretical model.

Keywords: *rotating cavity, rotating discs, fluid flow, heat transfer*

A rotating cylindrical cavity provides a simple model to study the flow and heat transfer between corotating turbine or compressor discs. A rotating cavity with an axial throughflow (where air enters the cavity through a central hole in one disc and leaves through the centre of the second disc) or a radial outflow (where air enters through a central hole in one disc and leaves through holes in the peripheral shroud) has been investigated by Owen and Bilimoria[1], Owen and Pincombe[2,3] and Owen and Onur[4]. In the work described in the two-part paper, of which this is the first part, the rotating cavity with radial inflow (Fig 1) has been studied.

A comprehensive analysis of isothermal laminar source-sink flow in a rotating cavity was made by Hide[5] who considered the case where the flow enters the cavity at radius $r=b$, through a uniform source, and leaves at radius $r=a$, through a uniform sink. The source region (Hide refers to a source 'layer', but for the current study this term seems inappropriate for a region that can, under certain conditions, extend throughout most of the cavity) divides the incoming flow from the source into two Ekman layers; the sink layer distributes the flow from the Ekman layers into the sink. Between the Ekman layers, the source region and the sink layer is an interior core of inviscid rotating fluid in which the radial and axial components of velocity are zero.

In addition to Hide's analysis, Bennetts and Jackson[6] and Chew, Owen and Pincombe[7] have conducted numerical analyses of the laminar flow case. Owen, Pincombe and Rogers[8] obtained solutions of the linear and the nonlinear Ekman layer equations, using integral momentum techniques, for source-sink flows in a rotating cavity. Their predictions of the tangential velocity inside a rotating cavity were found to be in good agreement with measured values over a wide range of laminar and turbulent conditions.

In this part of the paper, a simple model of the flow structure is discussed; the experimental apparatus is described; and flow visualization and measurements of the size of the source region are discussed. Part 2 includes comparisons between the theoretical and measured velocity profiles and pressure drops, together with measurements of the average Nusselt numbers when one of the discs is heated.

A simple model of the flow structure

Fig 1 shows a schematic diagram of the flow structure inside a rotating cylindrical cavity with a radial inflow of fluid. The flow enters at $r=b$, through a series of holes or a slot in the centre of the peripheral shroud, and leaves at $r=a$. In the source region, which extends for $r_e \leqslant r \leqslant b$, the incoming fluid is entrained into boundary layers on the discs and is then distributed into the two Ekman layers, which transport the fluid to the sink layer. Bounded by the source region, the Ekman layers and the sink layer, is the rotating inviscid interior core, where the radial and axial components of velocity are zero. The angular speed of the core is greater than that of the adjacent discs and depends on the flow rate in the Ekman layers.

The incoming fluid, which has to pass through the rotating shroud, enters the source region with a volumetric flow rate Q and with some initial swirl. Thus, at $r=b$, $V_\phi/\Omega b = c$, where V_ϕ is the tangential component of velocity of the fluid, relative to a stationary frame of reference, and c is the 'swirl fraction'. It is assumed that $0<c<1$; the actual value would be expected to depend on the shroud geometry, the rotational speed of the cavity

* School of Engineering and Applied Sciences, University of Sussex, Falmer, Brighton, Sussex, UK
Received 10 October 1984 and accepted for publication in final form on 13 May 1985

and the fluid flow rate. Within the source region, but outside the boundary layers on the discs and shroud, the angular momentum of the inflowing fluid is assumed to be conserved. This results in a free vortex in the source region, such that

$$V_\phi/\Omega r = cx^{-2} \tag{1}$$

where $x = r/b$.

Near the discs, the nonlinear inertial and centrifugal forces are often negligibly small compared with the linear Coriolis forces. Under these conditions, the boundary-layer equations, referred to a rotating frame of reference, reduce to a balance between viscous forces and Coriolis forces: the resulting equations are often called 'the linear Ekman-layer equations'. Owen, Pincombe and Rogers[8] obtained solutions for the integral form of these equations for both laminar and turbulent flow. From their solutions, the tangential component of velocity within the core, but outside the Ekman layers, can be expressed as

$$V_\phi/\Omega r = 1 - \lambda x^{-\alpha} \tag{2}$$

where $\alpha = 2$ and $\lambda = \lambda_L$ for laminar flow; and $\alpha = 13/8$ and $\lambda = \lambda_T$ for turbulent flow. The definitions of λ_L and λ_T are given in the Notation; it should be noted that the volumetric flow rate, Q, of the fluid inside the cavity is taken to be positive for radial outflow and negative for inflow.

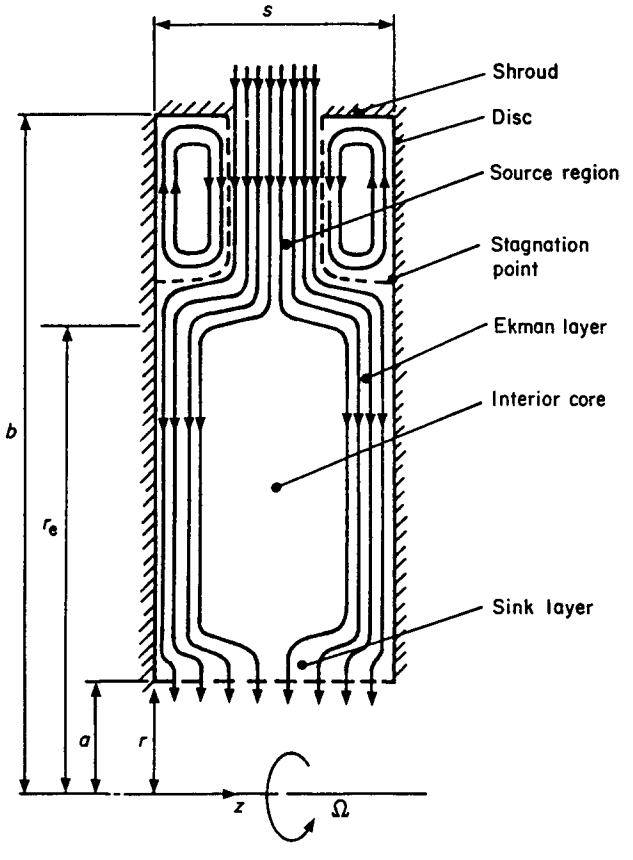

Fig 1 Schematic diagram of rotating cavity with radial inflow of fluid

Inside the source region the incoming fluid is gradually entrained into the inward-flowing boundary layers until, at some radius ($r = r_e$, say), all the fluid has been entrained. If, at radius r, the local volumetric flow rate in *each* Ekman layer is Q_l (where Q_l is negative for radial inflow), then $2|Q_l|$ if $r \geqslant r_e$. Outside the source region (for $r < r_e$ where $2Q_l = Q$), Eq (2) can be used to determine $V_\phi/\Omega r$. Inside the source region, where $V_\phi/\Omega r$ is given by Eq (1), Eq (2) can be employed to determine Q_l, such that

$$Q_l/vb = \pi Re_\phi^{1/2}(1 - cx^{-2})x^2 \tag{3}$$

for laminar flow, and

$$Q_l/vb = \mathrm{sgn}(1 - cx^{-2}) \times 0.140|1 - cx^{-2}|^{8/5} Re_\phi^{4/5} x^{13/5} \tag{4}$$

for turbulent flow. For both laminar and turbulent flow, there is a stagnation point on the disc (that is, $Q_l = 0$) when $x = c^{1/2}$. For values of x greater than this, where $V_\phi/\Omega r < 1$, there is radial outflow in the boundary layers; for smaller values of x, where $V_\phi/\Omega r > 1$, there is inflow. (The smoke patterns shown in some of the photographs taken during the flow visualization experiments were consistent with the occurrence of recirculation in the source region, caused by this reverse flow in the boundary layers.)

As $r = r_e$ (that is, $x = x_e$) when $2Q_l = Q$, it follows

Notation

- a Inner radius of disc
- b Outer radius of disc
- c Inlet swirl fraction
- C_w Flow rate coefficient $= Q/vb$
- Q Volumetric flow rate of fluid entering cavity
- Q_l Local volumetric flow rate in Ekman layer
- r Radial coordinate
- r_e Radius of edge of source region
- Re_r Radial Reynolds number $= C_w/2\pi x$
- Re_ϕ Rotational Reynolds number $= \Omega b^2/v$
- s Axial spacing between rotating discs
- V_ϕ Tangential component of velocity relative to a stationary reference frame
- x Dimensionless radial coordinate $= r/b$
- x_e Dimensionless radius of edge of source region $= r_e/b$
- z Axial coordinate
- β Volume expansion coefficient
- ΔT Temperature difference
- λ $= \lambda_L$ or λ_T for laminar or turbulent Ekman-layer flow
- λ_L $= (1/2\pi)C_w Re_\phi^{-1/2}$
- λ_T $= \mathrm{sgn}(Q)2.22|C_w|^{5/8} Re_\phi^{-1/2}$
- ν Kinematic viscosity
- ρ Density
- Ω Angular speed of cavity

Subscripts

- l Pertaining to local value
- L Pertaining to laminar flow
- T Pertaining to turbulent flow

from Eq (3) that

$$x_e=(c-|\lambda_L|)^{1/2} \tag{5}$$

for laminar flow, and from Eq (4) that

$$x_e=(c-|\lambda_T|x_e^{3/8})^{1/2} \tag{6}$$

for turbulent flow. It should be noted that Eqs (5) and (6) also correspond to the position of the intercepts of the curves defined by Eqs (1) and (2). By equating (5) and (6), it follows that the size of the source region for laminar Ekman-layer flow equals that for turbulent flow (if the fractional swirl of the incoming fluid is the same) when

$$|\lambda_L|=|\lambda_T|x_e^{3/8} \tag{7}$$

Using the definitions in the Notation, this occurs when $Re_r=180$; it was in fact proposed in Ref (8) that this equation can be used to estimate the position of the transition from laminar to turbulent Ekman-layer flow.

The experimental apparatus

The rotating-cavity rig

Fig 2 shows a simplified diagram of the rotating-cavity rig, which was a modified version of the rig used by Owen and Bilimoria[1] and Owen and Onur[4] for radial outflow experiments. As details of the rig can be found in the above references, only the salient features and the modifications for the inflow experiments are described below.

The cavity comprised two stainless steel discs of 762 mm diameter ($b=381$ mm) and a peripheral shroud. For the optical measurements, the shroud was made from polycarbonate of 1 mm thickness; for the heat transfer tests reported in Part 2, the shroud was made from paxolin of 1.5 mm thickness. The shroud was secured to the discs by means of circumferential loops of bowden cables; the ends of the cables were clamped to two bridges that were bolted, diametrically opposite each other, to the periphery of each disc. For the tests reported below, the axial spacing, s, between the discs was 51 mm.

Cooling air, which entered the cavity through holes or slots in the shroud, was extracted from the cavity through an annular hole of 76 mm outside diameter ($a/b=0.1$) and 25 mm inside diameter in the centre of one of the discs. Referring to Fig 2, air was extracted through the right-hand disc for most of the optical tests and through the left-hand disc (which permitted higher flow rates to be achieved) for the heat-transfer tests. The air was extracted by one or more centrifugal blowers, and the flow rate was measured by an orifice plate or, for the lower flow rates, an Annubar differential-pressure sensor. When air was extracted through the left-hand disc (as viewed in Fig 2) leakage occurred in the seals between the rotating and stationary components. This leakage, which was from the surrounding air into the (low pressure) cooling air downstream of the cavity itself, increased with increasing rotational speed; the results presented in this paper are corrected according to a calibration described by Owen, Pincombe and Firouzian[9]. The radial pressure drop across the cavity was measured using a static pressure tap, on the stationary piping downstream of the cavity, and a manometer (with a resolution of 1 mm wg); the air was admitted to the cavity at atmospheric pressure.

The cavity was rotated at speeds up to 2500 rev/min by an 11 kW thyristor-controlled dc motor; the speed was measured to an accuracy of one rev/min by a magnetic transducer, a 60-pole tachometer disc, and an electronic timer-counter. The outer 180 mm of the right-hand disc could be heated up to 100°C by thirty 750 W radiant 'firebar' elements; the power input to the heater bank was measured by a wattmeter.

The surface temperatures of the disc were measured by ten chromel-constantan thermocouples of 0.13 mm diameter embedded at radial intervals of 34 mm on each face of the discs. The signals were brought out via silver/silver graphite slipring units, and the voltages were

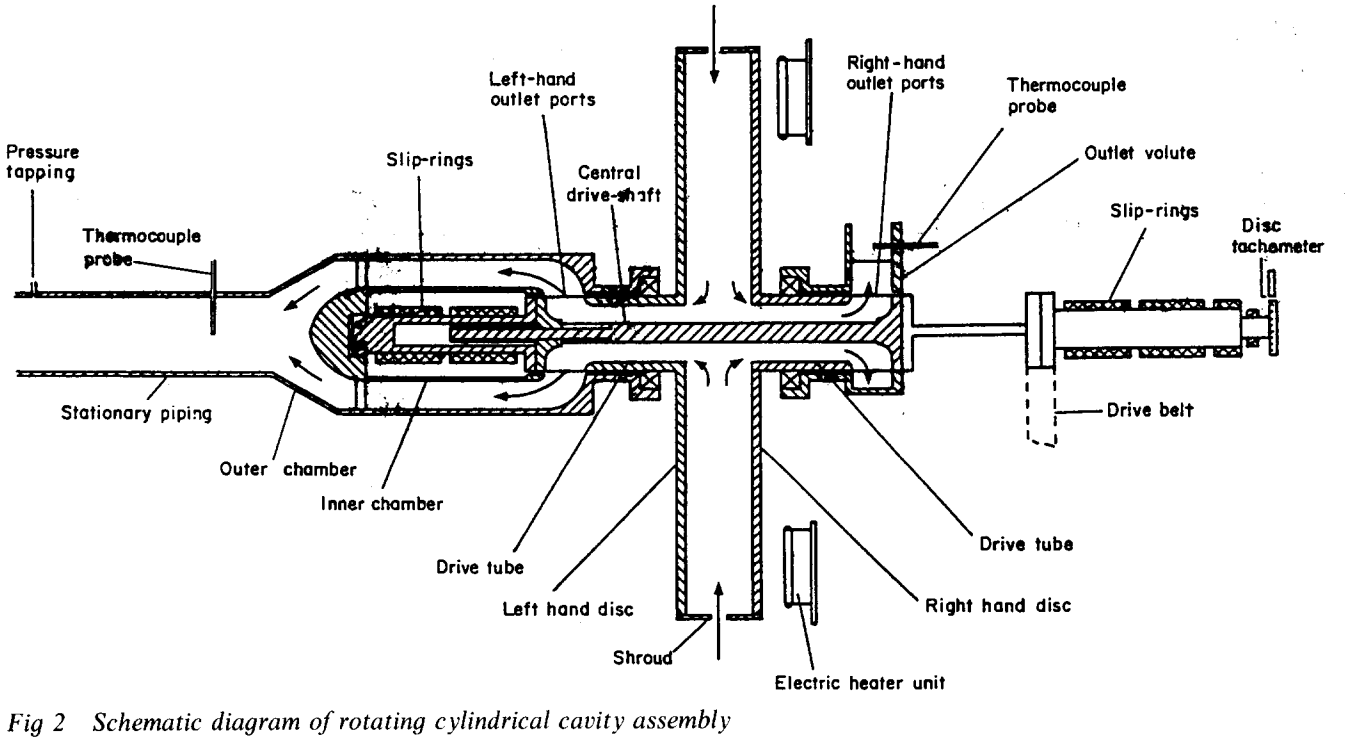

Fig 2 Schematic diagram of rotating cylindrical cavity assembly

read and recorded (to a resolution of 1 μV) by a Solartron data-logger. The inlet air static temperature was measured by means of a thermocouple probe, located on the horizontal centreline of the cavity, which could be traversed axially at a radial distance of 11 mm from the shroud. The outlet air temperature was measured by a probe which was traversed radially across the stationary piping downstream of the cavity.

Shroud geometry

A total of six different shroud geometries was tested. Shroud A (the 'central-inlet' shroud) contained 30 holes of 28.6 mm diameter spaced at 12° angular intervals on the mid-axial ($z/s=0.5$) plane. Shroud B (the 'twin-inlet' shroud) contained one row of 30 holes, of 20.6 mm diameter spaced at 12° angular intervals, adjacent to the inner surface of the heated disc, and a second row of 30 holes (displaced by 6° intervals from the first row) adjacent to the inner surface of the unheated disc. In shroud C (the 'side-inlet' shroud) the 30 holes of shroud B adjacent to the unheated disc were blanked off so that cooling air entered down the heated disc.

The above three shrouds were used for both heat transfer and for optical tests; the three shrouds described below were used only for optical tests. Shroud D (the 'small-hole' shroud) was similar to shroud A, but the hole diameter was 6.3 mm. Shroud E (the 'slotted-inlet' shroud) contained a continuous peripheral slot of 11 mm axial width, with the centre of the slot in the mid-axial plane. In shroud F (the 'foam-filled' shroud), a continuous peripheral slot of 5 mm axial width, covered with plastic foam (with a pore size of approximately $\frac{1}{2}$ mm diameter) of 10 mm radial thickness was used; this latter shroud was intended to produce 'solid-body rotation' of the fluid entering the cavity.

Optical instrumentation

For the flow visualization study, a flat beam of light was transmitted through the polycarbonate shroud and along the axis of rotation (referred to below as the r–z plane) by the use of a 4 W Spectra Physics argon-ion laser (operating in the all-line mode) and a cylindrical lens. The air immediately outside the cavity was 'seeded' by means of a Concept smoke generator, which produced 'clouds' of 0.8 μm-diameter oil particles. Photographs were obtained with a Canon A1 35 mm camera with motor drive; 400 ASA film was used at a rate up to five frames per second. Alternatively, the smoke patterns could be recorded using a Sony video camera and tape recorder, which had still and slow motion playback facilities. Further details of the optical instrumentation are given by Pincombe[10].

Flow visualization

Photographs obtained using the instrumentation described in the preceding section are shown in Fig 3 for isothermal flow with the 'central-inlet' shroud (shroud A); the r–z plane was illuminated by the Argon-ion laser ('looking' through the polycarbonate shroud). Oil vapour from the Concept smoke generator was pulsed into the air surrounding the cavity, where it condensed to form clouds of smoke. The smoke, which shows up as a white region in the photographs, was subsequently entrained into the cavity. The camera was mounted with its optical axis normal to the plane of illumination, and a series of photographs was taken from the time the smoke entered the cavity to the time when it had been convected to all regions of interest.

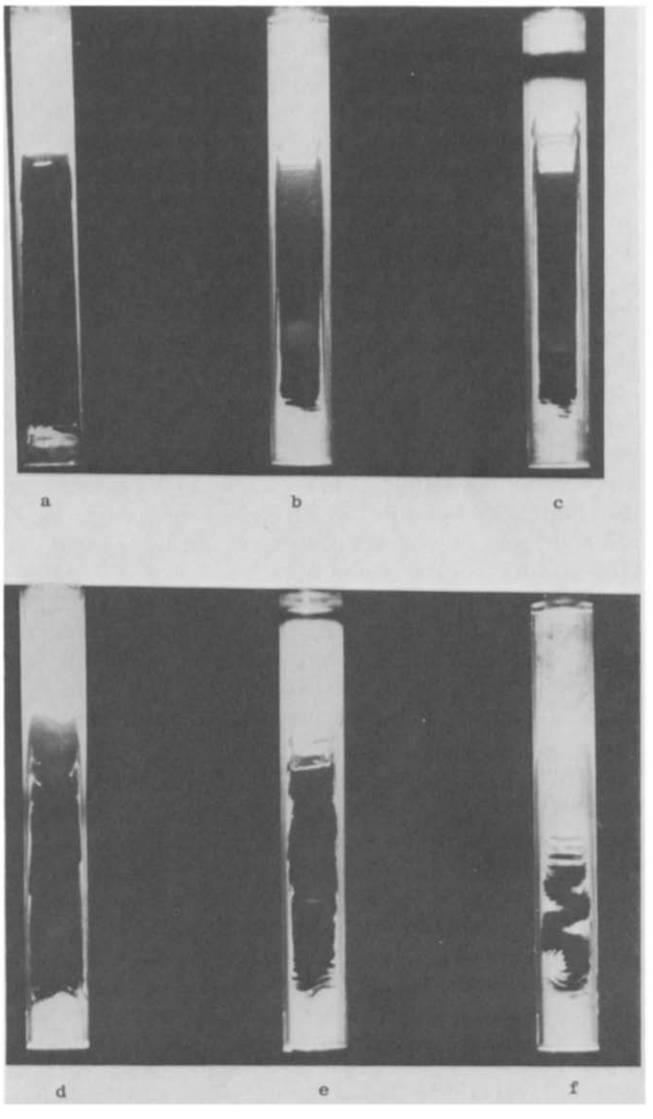

Fig 3 Flow visualization in the isothermal rotating cavity with shroud A for $\mathrm{Re}_\phi = 0.4 \times 10^5$: *(a), (b), (c)* $|C_w| = 96$; *(d), (e), (f)* $|C_w| = 310$

Figs 3a, b and c show a series of photographs taken for $Re_\phi = 0.4 \times 10^5$ and $|C_w| = 96$; flow enters at $x = 1$, on the top of photographs, and leaves at $x = 0.1$ ($r = a$) through the centre of the right-hand disc; the bottom of the photographs is at the centre-line of the cavity. The white source region, Ekman layers and sink layer stand out in contrast to the black interior core (where smoke penetrates slowly by diffusion rather than rapidly by convection). For $|C_w| = 96$, transition from laminar to turbulent flow occurs (for $Re_r = 180$) at $x = 0.085$; the flow should, therefore, be laminar throughout the cavity.

In Fig 3a, smoke has been convected from the source to the sink via the Ekman layers. At the time when Fig 3b was taken, smoke can be seen returning from the sink to the source via the 'outflow regions' of the

Ekman layers. This effect, which is predicted by laminar Ekman-layer theory*, has also been observed[3] for radial outflow in a rotating cavity. At a later time, Fig 3c shows that the smoke in the 'outflow regions' has reached the source region. (It should be pointed out that the black band across the source region in Fig 3c is caused by one of the two shroud-support bridges, attached to the periphery of each disc, passing through the field-of-view; this also occurs on some of the other photographs.)

Figs 3d, e and f show a series of photographs taken at the same rotational Reynolds number, $Re_\phi = 0.4 \times 10^5$, but at a higher flow rate, $|C_w| = 310$. For this value of C_w, transition from laminar to turbulent flow might be expected to occur in the Ekman layers at $x = 0.27$. Comparison between Figs 3d and 3a shows that an increase of $|C_w|$ is accompanied by an increase in the size of the source region and by the appearance of instabilities on the boundaries of the Ekman layers. In fact, at $Re_\phi = 0.4 \times 10^5$, the flow structure became unstable for $|C_w| > 180$ and the source region appeared to oscillate. When viewing the r–z plane, the size of the source region increased and decreased periodically in a non-axisymmetric fashion; Figs 3e and 3f show the approximate minimum and maximum sizes ($x_e \simeq 0.63$ and 0.43) of the source region during these oscillations.

At higher flow rates, the periodic behaviour sometimes spontaneously changed to a disordered or chaotic flow structure. For example, at $|C_w| = 400$ and $Re_\phi = 3 \times 10^5$ (the maximum Reynolds number used in the flow visualization tests), 'fingers' of smoke moved axially across the cavity from the Ekman layers into the interior core. A similar effect has been observed[3] during the transition from laminar to turbulent flow in the Ekman layers in a rotating cavity with radial outflow. However, for the inflow case considered here, where the flow was unsteady, the presence of the axial 'fingers' suggested that there was an imbalance of flow rate between the two Ekman layers, and that axial flow was necessary to redress the balance.

For a superimposed radial outflow (that is, where the net flow is from the centre of the cavity to the periphery), two independent conditions were found to cause chaotic flow. Firstly, isothermal tests with shrouds that had large holes (the ratio of hole area to total peripheral area being about one quarter) revealed that chaotic flow could occur at large rotational speeds. At these speeds, the pressure inside the cavity can become negative relative to the ambient air; as a consequence, ingress of ambient fluid occurs through the holes in the shroud. This ingested fluid flows radially inwards whilst the superimposed flow is outwards. Secondly, during tests in which one disc was heated, chaotic flow was also observed to occur at large rotational speeds. Under these conditions, buoyancy forces can cause a radial inflow of fluid, near the heated disc, in opposition to the superimposed outflow.

For a superimposed radial inflow, it was shown above that local outflow can occur in the boundary layers inside the source region (for $x > c^{1/2}$). Such outflow can only occur for $c < 1$; this, as is discussed in the following section, is the case for shrouds A to E. In fact, flow visualization confirmed the presence of outflow in the source region during tests with the perforated shrouds; for the foam-filled shroud F, where $c = 1$, outflow did not occur. It is, therefore, significant that, although flow instabilities were observed for shrouds A to E, no such instabilities were observed – over the range of parameters tested – for shroud F. It was also observed that heating one of the discs tended to delay the onset of instabilities; as buoyancy forces tend to oppose radial outflow on the hot disc, it would appear that, as noted above, a mixture of radial outflow and inflow inside a rotating cavity can destabilize the flow structure.

Fig 4 shows photographs taken during flow visualization, using shroud A, for $|C_w| = 400$ and $Re_\phi = 3 \times 10^5$ when one disc (the right-hand disc in the photographs) was heated to a maximum temperature of approximately 100°C ($\beta \Delta T \simeq 0.2$, where β is the volume expansion coefficient and ΔT is the maximum temperature difference between the disc and the inlet air, which was approximately 25°C); typical disc temperature profiles are shown in Part 2. Owing to the use of radiant heaters, the disc temperature was not uniform: the maximum temperature occurred at $x \simeq 0.8$. Although the flow structure was disordered during isothermal radial inflow, heating one disc tended to stabilize the flow (although instability sometimes appeared at higher flow rates); this is in contrast to the radial outflow case where heating one disc destabilized the flow. Buoyancy effects tend to create inflow near a hot rotating disc, and this may reduce the outflow (for $x > c^{1/2}$) in the source region.

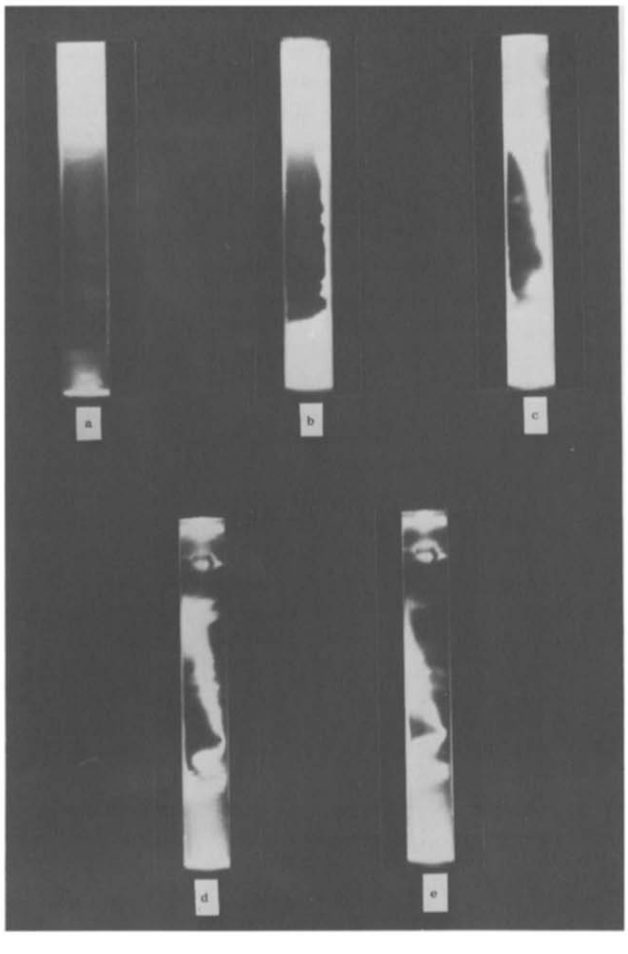

Fig 4 Flow visualization in the heated rotating cavity with shroud A for $|C_w| = 400$, $Re_\phi = 3 \times 10^5$ and $\beta \Delta T \simeq 0.2$

* For laminar flows, the component of radial velocity inside the Ekman layer is described by an exponentially-decaying sinewave: there are alternate regions of inflow and outflow

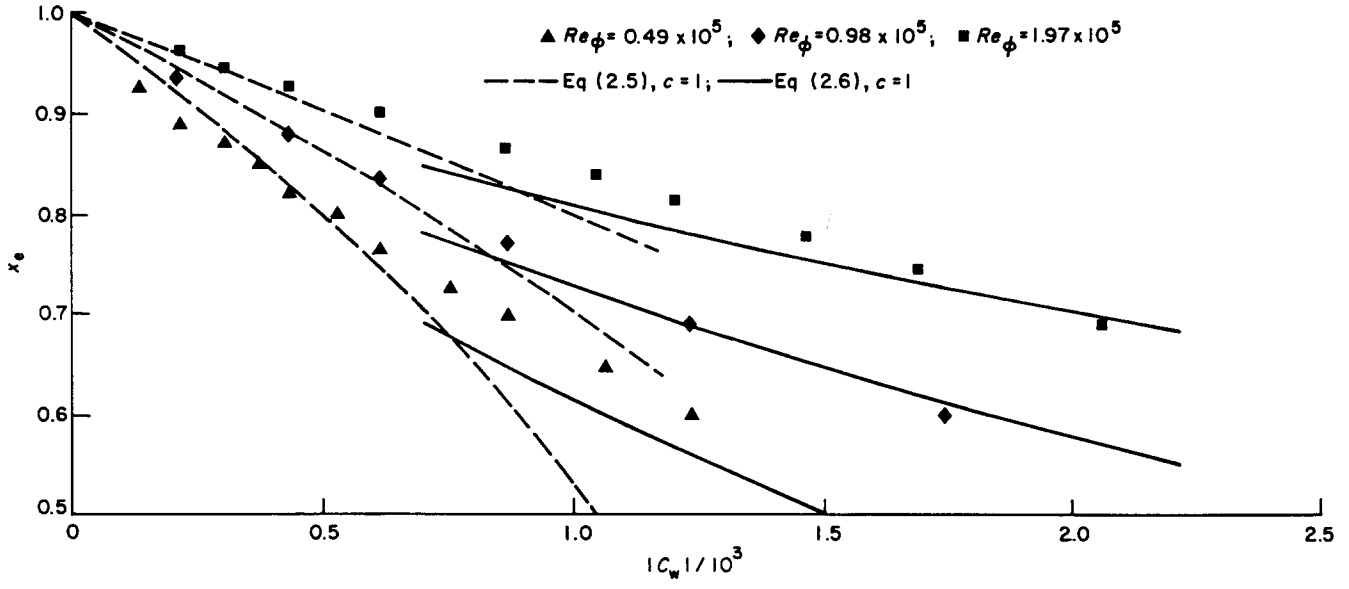

Fig 5 Variation of radial extent of source region with flow rate for shroud F

In Fig. 4a, the smoke has been convected from the source region to the sink layer: the Ekman layers are just visible. Figs 4b, c, d and e were respectively taken 4, 9, 12 and 17 seconds later; this sequence suggests that there is an 'axial wind' as flow moves progressively from the hot (right-hand) disc towards the cold disc. It should be noted that the flow is expected to be laminar (for $Re_r < 180$) for $x > 0.35$, and the observation of an axial wind is consistent with the numerical analysis of Chew[11]. He showed that, for laminar flow in which buoyancy effects are significant, the axial wind depends on the expression $r^2 \Delta T$, where ΔT is the axial temperature difference between the hot and the cold discs: if $r^2 \Delta T$ increases with increasing radius, the axial wind is from the hot to the cold disc, and vice versa.

Measurement of the extent of the source region

For isothermal flow, tests were conducted with five of the shrouds referred to above (shroud E was not tested) for $0 \leqslant C_w \leqslant 2000$ and $0.5 \leqslant Re_\phi/10^5 \leqslant 10$. In these tests, the radial extent of the source region was determined by flow visualization: the r–z plane was illuminated, and smoke was pulsed into the cavity. By using the video monitor, it was possible to measure the radial location, r_e, of the edge of the source region to an estimated resolution of 2% of the radius of the cavity. However, the overall accuracy of these measurements was affected by the time taken for the smoke to diffuse and by the unsteadiness of the flow. For unsteady conditions, which often occurred for tests with the perforated shrouds, the minimum and maximum radii of the oscillating source region were determined from a frame-to-frame playback of the video recorder; r_e was taken to be the arithmetic mean of these radii. No attempt was made to determine r_e under the chaotic conditions referred to in the previous section.

For all the shrouds tested, it was found that x_e (where $x_e = r_e/b$) decreased with increasing $|C_w|$ and with decreasing Re_ϕ. For the perforated shrouds A, B, C and D, the extent of the source region appeared to be only weakly dependent on the inlet geometry; for the 'foam-filled' shroud F, the source region was significantly smaller (that is, x_e was larger) than that of the other shrouds. For all the tests, the size of the sink layer appeared to be independent of shroud geometry, rotational speed and flow rate; the layer extended to $x \simeq 0.15$.

Fig 5 shows, for shroud F, the variation of the measured values of x_e with $|C_w|$ for $Re_\phi/10^5 = 0.49$, 0.98 and 1.97. This foam-filled shroud was intended to produce solid-body rotation of the flow at inlet to the cavity; Eqs (5) and (6) (with $c = 1$) are also included in Fig 5. As stated above, the intercept of the curves defined by these equations occurs at $Re_r = 180$, which marks the transition from laminar to turbulent flow in the Ekman layers. Bearing in mind the simplicity of the model, the agreement between the theoretical and measured values is reasonable.

The data for the perforated shrouds A, B, C and D were correlated using Eq (5) with $c = 0.54$ for $Re_r < 180$, and using Eq (6) with $c = 0.59$ for $Re_r > 180$. Fig 6 shows, for the four perforated shrouds and shroud F, the variation of x_e with (a) $|\lambda_L|$, for $Re_r < 180$, and (b) $|\lambda_T|$, for $Re_r > 180$. Also included are Eqs (5) and (6) with the appropriate values of c. Apart from the scatter (which is worse for the perforated shrouds, where unsteadiness made measurements difficult), the agreement between the theoretical and experimental values is good.

The above results support the arguments used above about the structure of the flow in the source region; more support is provided by the velocity measurements presented in Part 2. The fact that a value of $c = 1$ fits the data for the foam-filled shroud F is not surprising: this shroud was expected to generate solid-body rotation at the inlet to the cavity. However, the fact that, for the perforated shrouds, a single value of c ($c = 0.54$) fits the laminar flow data and a single value ($c = 0.59$) fits the turbulent flow data (over a wide range of flow rates, rotational speeds and shroud geometries) is surprising. It appears to suggest that for perforated shrouds with holes of small 'length-to-diameter ratio' (the 'l/d ratio' where l is the shroud thickness and d the hole diameter, was less than 0.2 for the shrouds tested), flow enters the cavity with a 'swirl fraction' of just over one half; for the foam-filled shroud (with an effective 'l/d ratio' greater than twenty,

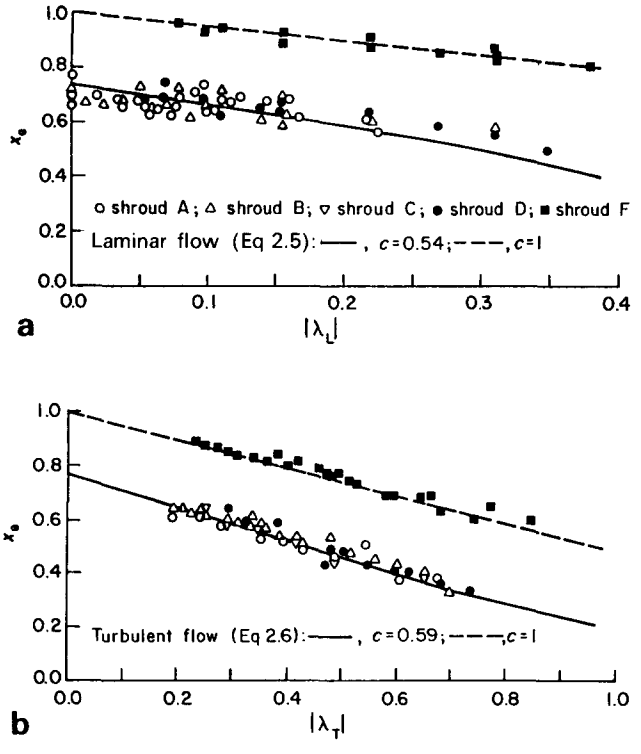

Fig 6 Variation of radial extent of the source region with λ

where l is the thickness of the foam), the swirl fraction is unity.

Conclusions

Flow visualization has been used to study the flow structure in a rotating cylindrical cavity, comprising two steel discs and a peripheral polycarbonate shroud, with a radial inflow of fluid. Each disc had an inner to outer radius ratio of $a/b=0.1$, and the cavity had an axial distance to outer radius ratio of $s/b=0.133$. Measurements were made to determine the radial extent of the source region for dimensionless flow rates of air up to $|C_w| \simeq 2000$ and rotational Reynolds numbers up to $Re_\phi \simeq 10^6$. For these tests, five different shroud geometries were used: four 'perforated' shrouds, with a series of discrete holes, and a 'foam-filled' shroud, with a circumferential foam-filled slot in the centre of the shroud.

The flow visualization confirmed the expected flow structure: a source region near the shroud, Ekman layers on the discs, a sink layer near the centre of the cavity, and an interior core of rotating fluid. Although, for one of the perforated shrouds, the structure could be destabilized above a critical value of $|C_w|$, heating one disc tended to stabilize the flow. During heating an 'axial wind' was observed to transport fluid from the hot to the cold disc.

By defining the edge of the source region as the radius at which all fluid entering the cavity has been entrained into the (laminar or turbulent) Ekman layers, and by assuming that free-vortex flow occurs outside these layers, the radial extent of the source region has been estimated. The theoretical estimates are in good agreement with experimental measurements if the 'swirl fraction' (that is, the ratio of the angular speed of the fluid entering the cavity to that of the shroud) is assumed to be just over half for the 'perforated shrouds' and unity for the 'foam-filled' shroud.

References

1. **Owen J. M. and Bilimoria E. D.** Heat transfer in rotating cylindrical cavities. *J. Mech. Engng Sci. 1977*, **19**, *175*
2. **Owen J. M. and Pincombe J. R.** Vortex breakdown in a rotating cylindrical cavity. *J. Fluid Mech. 1979*, **90**, *109*
3. **Owen J. M. and Pincombe J. R.** Velocity measurements inside a rotating cylindrical cavity with a radial outflow of fluid. *J. Fluid Mech. 1980*, **99**, *111*
4. **Owen J. M. and Onur H. S.** Convective heat transfer in a rotating cylindrical cavity. *J. Engng Power, 1983*, **105**, *178*
5. **Hide R.** On source-sink flows in a rotating fluid. *J. Fluid Mech., 1968*, **32**, *737*
6. **Bennetts D. A. and Jackson W. D. N.** Source-sink flows in a rotating annulus: a combined laboratory and numerical study. *J. Fluid Mech. 1974*, **66**, *689*
7. **Chew J. W., Owen J. M. and Pincombe J. R.** Numerical predictions for laminar source-sink flow in a rotating cavity. *J. Fluid Mech. 1984*, **143**, *451*
8. **Owen J. M., Pincombe J. R. and Rogers R. H.** Source-sink flow inside a rotating cavity. *J. Fluid Mech. 1985*, **155**, *233*
9. **Owen J. M., Pincombe J. R. and Firouzian M.** *Heat transfer and fluid flow in a rotating cavity with a radial inflow of coolant. Part 1: Measurements with a central-inlet shroud. Report No. 80/TFMRC/19, 1980, School of Engng and Appl. Sciences, University of Sussex, UK*
10. **Pincombe J. R.** *Optical measurements of the flow inside a rotating cylinder. D.Phil. thesis, 1983, University of Sussex, UK*
11. **Chew J. W.** *Computation of flow and heat transfer in rotating cavities. D.Phil. thesis, 1982, University of Sussex, UK*